Northumbria Research Link

www.northumbria.ac.uk/nrl

northumbria
UNIVERSITY
University Library

Geometrically nonlinear theory of thin-walled composite box beams using shear-deformable beam theory

Thuc Phuong Vo* and Jaehong Lee†

Department of Architectural Engineering, Sejong University
98 Kunja Dong, Kwangjin Ku, Seoul 143-747, Korea

(Dated: September 4, 2009)

A general geometrically nonlinear model for thin-walled composite space beams with arbitrary lay-ups under various types of loadings is presented. This model is based on the first-order shear deformable beam theory, and accounts for all the structural coupling coming from both material anisotropy and geometric nonlinearity. The nonlinear governing equations are derived and solved by means of an incremental Newton-Raphson method. A displacement-based one-dimensional finite element model that accounts for the geometric nonlinearity in the von Kármán sense is developed. Numerical results are obtained for thin-walled composite box beams under vertical load to investigate the effects of shear deformation, geometric nonlinearity and fiber orientation on axial-flexural-torsional response.

Keywords: Thin-walled composite beams; shear deformation; axial-flexural-torsional response; nonlinear theory.

I. INTRODUCTION

Fiber-reinforced composite materials have been used over the past few decades in a variety of structures. Composites have many desirable characteristics, such as high ratio of stiffness and strength to weight, corrosion resistance and magnetic transparency. Thin-walled structural shapes made up of composite materials, which are usually produced by pultrusion, are being increasingly used in many engineering fields.

The theory of thin-walled closed section members made of isotropic materials was first developed by Vlasov [1]

―――――

*Graduate student

†Professor, corresponding author. Tel.:+82-2-3408-3287; fax:+82-2-3408-3331

; Electronic address: `jhlee@sejong.ac.kr`

and Gjelsvik [2]. A large number of practical problems require a geometrically nonlinear formulation, such as the postbuckling behavior, load carrying capacity of structures used in aeronautical, aerospace as well as in mechanical and civil engineering. Thin-walled composite structures are often very thin and have complicated material anisotropy. The studies of these structures carried out so far may broadly be divided into two groups. The first and most common approach is based on an analytical technique, while the other approach requires a two-dimensional finite element analysis to obtain the cross-section stiffness matrix. Atilgan and Hodges et al. [3,4] pioneered the second approach, which was referred to as the so-called "Variational Asymptotic Beam Section Analysis" (VABS). VABS used the variational asymptotic method (VAM) to split a three-dimensional nonlinear elasticity problem into a two-dimensional linear cross-sectional analysis and a one-dimensional, nonlinear beam problem. Hodges and co-workers (e.g., Cesnik et al. [5,6], Volovoi et al. [7], Yu et al. [8]) further applied the concept introduced by VAM to two dimensional cross-sectional problem and derived closed-form expressions for the cross-sectional stiffness coefficients of thin-walled beams. By using Atilgan and Hodges's beam model, Jeon et al. [9] developed an analysis model of large deflection for the static and dynamic analysis of composite box beams.

In the present investigation, an analytical approach is adopted for the derivation of the cross-sectional stiffness matrix considering different effects and their coupling to yield a general formulation. Bauld and Tzeng [10] presented nonlinear model for thin-walled composite beams by extending Gjelsvik's formulation to the balanced symmetric laminated composite materials. However, the formulation was somewhat not consistent in the sense that it used coordinate mapping when developing nonlinear stresses instead of variational formulation. A finite element formulation was developed by Stemple and Lee [11,12] to take into account the warping effect of composite beams undergoing large deflection or finite rotation. Kalfon and Rand [13] derived the nonlinear theoretical modeling of laminated thin-walled composite helicopter rotor blades. The derivation was based on nonlinear geometry with a detailed treatment of the body loads in the axial direction which were induced by the rotation. Pai and Nayfeh [14] developed a fully nonlinear theory of curved and twisted composite rotor blades. The theory accounted for warping due to bending, extensional, shearing and torsional loadings, and three-dimensional stress effects by using the results of a two-dimensional, static, sectional, finite element analysis. Bhaskar and Librescu et al. [15,16] developed non-linear theory of thin-walled composite beams, which was employed in a broad field of engineering problems. In this model, the transverse shear deformation was taken into account but the warping torsion component was neglected. Special attention deserved the works of Machado, Cortinez and Piovan [17-19] who introduced a geometrically non-linear theory for thin-walled composite beams for both open and closed cross-sections and took into account shear flexibility

(bending and warping shear). This non-linear formulation was developed by using a non-linear displacement field, whose rotations were based on the rule of semi-tangential transformation. It was used for analyzing the stability of thin-walled composite beams with general cross-section. By using a geometrically higher-order non-linear beam theory, Machado [19] investigated the influence of large rotations on the buckling and free vibration behavior of thin-walled composite beam. However, it was strictly valid for symmetric balanced laminates and especially orthotropic laminates. Recently, Sapountzakis and Panagos [20] introduced the non-linear analysis of a composite Timoshenko beam with arbitrary variable cross section undergoing moderate large deflections by employing the analog equation method (AEM), a BEM-based method.

In this paper, which is an extension of the authors' previous works [21-25], a geometrically nonlinear model for thin-walled composite beams with arbitrary lay-ups under various types of loadings is presented. This model is based on the first-order shear deformable beam theory, and accounts for all the structural coupling coming from both material anisotropy and geometric nonlinearity. The general nonlinear governing equations are derived and solved by means of an incremental Newton-Raphson method. A displacement-based one-dimensional finite element model that accounts for the geometric nonlinearity in the von Kármán sense is developed. Numerical results are obtained for thin-walled composite box beam under vertical load to investigate the effects of shear deformation, geometric nonlinearity, fiber orientation, laminate stacking sequence and load parameter on axial-flexural-torsional response.

II. KINEMATICS

The theoretical developments presented in this paper require two sets of coordinate systems which are mutually interrelated. The first coordinate system is the orthogonal Cartesian coordinate system (x, y, z), for which the x and y axes lie in the plane of the cross section and the z axis parallel to the longitudinal axis of the beam. The second coordinate system is the local plate coordinate (n, s, z) as shown in Fig.1, wherein the n axis is normal to the middle surface of a plate element, the s axis is tangent to the middle surface and is directed along the contour line of the cross section. The (n, s, z) and (x, y, z) coordinate systems are related through an angle of orientation θ. As defined in Fig.1 a point P, called the pole, is placed at an arbitrary point x_p, y_p. A line through P parallel to the z axis is called the pole axis.

To derive the analytical model for a thin-walled composite beam, the following assumptions are made

1. The contour of the thin wall does not deform in its own plane.

2. Transverse shear strains $\gamma_{xz}^\circ, \gamma_{yz}^\circ$ and warping shear γ_ω° are incorporated. It is assumed that they are uniform over the cross-sections.

3. The linear shear strain $\bar\gamma_{sz}$ of the middle surface is to have the same distribution in the contour direction as it does in the St. Venant torsion in each element.

According to assumption 1, the midsurface displacement components $\bar u, \bar v$ at a point A in the contour coordinate system can be expressed in terms of a displacements U, V of the pole P in the x, y directions, respectively, and the rotation angle Φ about the pole axis

$$\bar u(s, z) = U(z)\sin\theta(s) - V(z)\cos\theta(s) - \Phi(z)q(s) \tag{1a}$$

$$\bar v(s, z) = U(z)\cos\theta(s) + V(z)\sin\theta(s) + \Phi(z)r(s) \tag{1b}$$

These equations apply to the whole contour. The out-of-plane shell displacement $\bar w$ can now be found from the assumption 2. For each element of middle surface, the midsurface shear strains in the contour can be expressed with respect to the transverse shear and the warping shear strains

$$\bar\gamma_{nz}(s, z) = \gamma_{xz}^\circ(z)\sin\theta(s) - \gamma_{yz}^\circ(z)\cos\theta(s) + \gamma_\omega^\circ(z)q(s) \tag{2a}$$

$$\bar\gamma_{sz}(s, z) = \gamma_{xz}^\circ(z)\cos\theta(s) + \gamma_{yz}^\circ(z)\sin\theta(s) - \gamma_\omega^\circ(z)r(s) - \left[\gamma_\omega^\circ(z) - \Phi'(z)\right]\frac{F(s)}{t(s)} \tag{2b}$$

where $t(s)$ is the thickness of contour box section, $F(s)$ is the St. Venant circuit shear flow. Further, it is assumed that midsurface shear strain in $s - n$ direction is zero ($\bar\gamma_{sn} = 0$). From the definition of the shear strain, $\bar\gamma_{sz}$ can also be given for each element of middle surface as

$$\bar\gamma_{sz}(s, z) = \frac{\partial\bar v}{\partial z} + \frac{\partial\bar w}{\partial s} \tag{3}$$

After substituting for $\bar v$ from Eq.(1) into Eq.(3) and considering the following geometric relations

$$dx = ds\cos\theta \tag{4a}$$

$$dy = ds\sin\theta \tag{4b}$$

Displacement $\bar w$ can be integrated with respect to s from the origin to an arbitrary point on the contour

$$\bar w(s, z) = W(z) + \Psi_y(z)x(s) + \Psi_x(z)y(s) + \Psi_\omega(z)\omega(s) \tag{5}$$

where Ψ_x, Ψ_y and Ψ_ω represent rotations of the cross section with respect to x, y and ω, respectively, given by

$$\Psi_y = \gamma^\circ_{xz}(z) - U' \tag{6a}$$

$$\Psi_x = \gamma^\circ_{yz}(z) - V' \tag{6b}$$

$$\Psi_\omega = \gamma^\circ_\omega(z) - \Phi' \tag{6c}$$

When the transverse shear effect is ignored, Eq.(6) degenerates to $\Psi_y = -U'$, $\Psi_x = -V'$ and $\Psi_\omega = -\Phi'$, and as a result, the number of unknown variables reduces to four leading to the Euler-Bernoulli beam model. The prime ($'$) is used to indicate differentiation with respect to z; and ω is the so-called sectorial coordinate or warping function given by

$$\omega(s) = \int_{s_\circ}^s \left[r(s) - \frac{F(s)}{t(s)} \right] ds \tag{7a}$$

$$\oint_i \frac{F(s)}{t(s)} ds = 2A_i \quad i = 1, ..., n \tag{7b}$$

where $r(s)$ is height of a triangle with the base ds; A_i is the area circumscribed by the contour of the i circuit. The explicit forms of $\omega(s)$, $F(s)$ for box section are given in the Appendix of Ref.[22].

The displacement components u, v, w representing the deformation of any generic point on the profile section are given with respect to the midsurface displacements $\bar{u}, \bar{v}, \bar{w}$ by assuming the first order variation of inplane displacements v, w through the thickness of the contour as

$$u(s, z, n) = \bar{u}(s, z) \tag{8a}$$

$$v(s, z, n) = \bar{v}(s, z) + n\bar{\psi}_s(s, z) \tag{8b}$$

$$w(s, z, n) = \bar{w}(s, z) + n\bar{\psi}_z(s, z) \tag{8c}$$

where, $\bar{\psi}_s$ and $\bar{\psi}_z$ denote the rotations of a transverse normal about the z and s axis, respectively. These functions can be determined by considering that the midsurface shear strains γ_{nz} is given by definition

$$\bar{\gamma}_{nz}(s, z) = \frac{\partial \bar{w}}{\partial n} + \frac{\partial \bar{u}}{\partial z} \tag{9}$$

By comparing Eq.(2) and (9), the function can $\bar{\psi}_z$ can be written as

$$\bar{\psi}_z = \Psi_y \sin\theta - \Psi_x \cos\theta - \Psi_\omega q \tag{10}$$

Similarly, using the assumption that the shear strain γ_{sn} should vanish at midsurface, the function $\bar{\psi}_s$ can be obtained

$$\bar{\psi}_s = -\frac{\partial \bar{u}}{\partial s} \tag{11}$$

The von Kármán type strains, in which only the products of u, v, and their derivatives are retained and all other nonlinear terms are neglected are given by

$$\epsilon_z(s, z, n) = \frac{\partial w}{\partial z} + \frac{1}{2}\left[\left(\frac{\partial u}{\partial z}\right)^2 + \left(\frac{\partial v}{\partial z}\right)^2\right] \tag{12a}$$

$$\gamma_{sz}(s, z, n) = \frac{\partial v}{\partial z} + \frac{\partial w}{\partial s} \tag{12b}$$

$$\gamma_{nz}(s, z, n) = \frac{\partial w}{\partial n} + \frac{\partial u}{\partial z} \tag{12c}$$

By substituting Eqs.(1), (5) and (8) into Eq.(12), and using the following relations

$$x - x_p = q\cos\theta + r\sin\theta \tag{13a}$$

$$y - y_p = q\sin\theta - r\cos\theta \tag{13b}$$

Eq.(12) can be rewritten as

$$\epsilon_z = \bar{\epsilon}_z + n\bar{\kappa}_z + n^2\bar{\chi}_z \tag{14a}$$

$$\gamma_{sz} = \bar{\gamma}_{sz} + n\bar{\kappa}_{sz} \tag{14b}$$

$$\gamma_{nz} = \bar{\gamma}_{nz} + n\bar{\kappa}_{nz} \tag{14c}$$

where

$$\bar{\epsilon}_z = \frac{\partial \bar{w}}{\partial z} + \frac{1}{2}\left[\left(\frac{\partial \bar{u}}{\partial z}\right)^2 + \left(\frac{\partial \bar{v}}{\partial z}\right)^2\right] \tag{15a}$$

$$\bar{\kappa}_z = -\frac{\partial^2 \bar{u}}{\partial z^2} - 2\frac{\partial^2 \bar{u}}{\partial s\partial z}\frac{\partial \bar{v}}{\partial z} \tag{15b}$$

$$\bar{\kappa}_{sz} = -2\frac{\partial^2 \bar{u}}{\partial s\partial z} \tag{15c}$$

$$\bar{\chi}_z = \left(\frac{\partial^2 \bar{u}}{\partial s\partial z}\right)^2 \tag{15d}$$

In Eq.(15), $\bar{\epsilon}_z, \bar{\kappa}_z, \bar{\kappa}_{sz}$ and $\bar{\chi}_z$ are midsurface axial strain and biaxial curvature of the shell, respectively. The above shell strains can be converted to beam strain components by substituting Eqs.(1), (5) and (8) into Eq.(15) as

$$\bar{\epsilon}_z = \epsilon_z^\circ + x\kappa_y + y\kappa_x + \omega\kappa_\omega \tag{16a}$$

$$\bar{\kappa}_z = \kappa_y\sin\theta - \kappa_x\cos\theta - \kappa_\omega q + 2\chi_z r \tag{16b}$$

$$\bar{\kappa}_{sz} = \kappa_{sz} \tag{16c}$$

$$\bar{\chi}_z = \chi_z \tag{16d}$$

where $\epsilon_z^\circ, \kappa_x, \kappa_y, \kappa_\omega, \kappa_{sz}$ and χ_z are axial strain, biaxial curvatures in the x and y direction, warping curvature with

respect to the shear center, twisting and high order curvature in the beam, respectively defined as

$$\epsilon_z^\circ = W' + \frac{1}{2}\left[U'^2 + V'^2 + (r^2 + q^2)\Phi'^2\right] - x_p V'\Phi' + y_p U'\Phi' \tag{17a}$$

$$\kappa_x = \Psi_x' - U'\Phi' \tag{17b}$$

$$\kappa_y = \Psi_y' + V'\Phi' \tag{17c}$$

$$\kappa_\omega = \Psi_\omega' \tag{17d}$$

$$\kappa_{sz} = \Phi' - \Psi_\omega \tag{17e}$$

$$\chi_z = \frac{1}{2}\Phi'^2 \tag{17f}$$

The resulting strains can be obtained from Eqs.(14) and (16) as

$$\epsilon_z = \epsilon_z^\circ + (x + n\sin\theta)\kappa_y + (y - n\cos\theta)\kappa_x + (\omega - nq)\kappa_\omega + (2rn + n^2)\chi_z \tag{18a}$$

$$\gamma_{sz} = \gamma_{xz}^\circ \cos\theta + \gamma_{yz}^\circ \sin\theta + \gamma_\omega^\circ(r - \frac{F}{2t}) + \kappa_{sz}(n + \frac{F}{2t}) \tag{18b}$$

$$\gamma_{nz} = \gamma_{xz}^\circ \sin\theta - \gamma_{yz}^\circ \cos\theta - \gamma_\omega^\circ q \tag{18c}$$

III. VARIATIONAL FORMULATION

Total potential energy of the system is calculated by sum of strain energy and potential energy

$$\Pi = \mathcal{U} + \mathcal{V} \tag{19}$$

where $\mathcal{U}$ is the strain energy

$$\mathcal{U} = \frac{1}{2}\int_v (\sigma_z\epsilon_z + \sigma_{sz}\gamma_{sz} + \sigma_{nz}\gamma_{sz})dv \tag{20}$$

The strain energy is calculated by substituting Eq.(18) into Eq.(20)

$$\mathcal{U} = \frac{1}{2}\int_v \left\{\sigma_z\left[\epsilon_z^\circ + (x + n\sin\theta)\kappa_y + (y - n\cos\theta)\kappa_x + (\omega - nq)\kappa_\omega + (2rn + n^2)\chi_z\right]\right.$$
$$+ \left.\sigma_{sz}\left[\gamma_{xz}^\circ \cos\theta + \gamma_{yz}^\circ \sin\theta + \gamma_\omega^\circ(r - \frac{F}{2t}) + \kappa_{sz}(n + \frac{F}{2t})\right] + \sigma_{nz}\left[\gamma_{xz}^\circ \sin\theta - \gamma_{yz}^\circ \cos\theta - \gamma_\omega^\circ q\right]\right\}dv \tag{21}$$

The variation of the strain energy, Eq.(21), can be stated as

$$\delta\mathcal{U} = \int_0^l (N_z\delta\epsilon_z + M_y\delta\kappa_y + M_x\delta\kappa_x + M_\omega\delta\kappa_\omega + V_x\delta\gamma_{xz}^\circ + V_y\delta\gamma_{yz}^\circ + T\delta\gamma_\omega^\circ + M_t\delta\kappa_{sz} + R_z\delta\chi_z)ds \tag{22}$$

where $N_z, M_x, M_y, M_\omega, V_x, V_y, T, M_t, R_z$ are axial force, bending moments in the x and y directions, warping moment (bimoment), shear force in the x and y directions, warping torque, torsional moment and the high order stress resultant with respect to the centroid respectively, defined by integrating over the cross-sectional area A as

$$N_z = \int_A \sigma_z \, ds \, dn \tag{23a}$$

$$M_y = \int_A \sigma_z (x + n\sin\theta) \, ds \, dn \tag{23b}$$

$$M_x = \int_A \sigma_z (y - n\cos\theta) \, ds \, dn \tag{23c}$$

$$M_\omega = \int_A \sigma_z (\omega - nq) \, ds \, dn \tag{23d}$$

$$V_x = \int_A (\sigma_{sz}\cos\theta + \sigma_{nz}\sin\theta) \, ds \, dn \tag{23e}$$

$$V_y = \int_A (\sigma_{sz}\sin\theta - \sigma_{nz}\cos\theta) \, ds \, dn \tag{23f}$$

$$T = \int_A \left[\sigma_{sz}(r - \frac{F}{2t}) - \sigma_{nz}q \right] ds \, dn \tag{23g}$$

$$M_t = \int_A \sigma_{sz}(n + \frac{F}{2t}) \, ds \, dn \tag{23h}$$

$$R_z = \int_A \sigma_z (2rn + n^2) \, ds \, dn \tag{23i}$$

The variation of the strain energy can be obtained by substituting Eqs.(17) and (18) into Eq.(22)

$$
\begin{aligned}
\delta\mathcal{U} = \int_0^l & \Big[N_z\delta W' + M_y\delta\Psi'_y + M_x\delta\Psi'_x + M_\omega\delta\Psi'_\omega + V_x\delta(U' + \Psi_y) + V_y\delta(V' + \Psi_x) \\
& + T\delta(\Phi' + \Psi_\omega) + M_t\delta(\Phi' - \Psi_\omega) + N_z(U'\delta U' + V'\delta V') \\
& + (M_y - x_p N_z)(V'\delta\Phi' + \Phi'\delta V') - (M_x - y_p N_z)(U'\delta\Phi' + \Phi'\delta U') + (r_p^2 N_z + R_z)\Phi'\delta\Phi' \Big] dz
\end{aligned}
\tag{24}
$$

On the other hand, the variation of work done by external forces can be written as

$$\delta\mathcal{V} = -\int_v (p_z\delta w + p_n\delta u + p_s\delta v) \, dv \tag{25}$$

where p_z, p_n, p_s are forces acting in z, n and s direction. The above expression can be written with respect to the shell forces and displacements by using Eq.(8)

$$\delta\mathcal{V} = -\int_0^l \int_s (\bar{p}_z\delta\bar{w} + \bar{p}_n\delta\bar{u} + \bar{p}_s\delta\bar{v} + \bar{m}_z\bar{\psi}_z + \bar{m}_s\bar{\psi}_s) \, ds \, dz \tag{26}$$

where $\bar{p}_z, \bar{p}_s, \bar{m}_z, \bar{m}_s, \bar{p}_n$ are shell forces defined by

$$(\bar{p}_z, \bar{m}_z) = \int_n p_z(1, n) \, dn \tag{27a}$$

$$(\bar{p}_s, \bar{m}_s) = \int_n p_s(1, n) \, dn \tag{27b}$$

$$\bar{p}_n = \int_n p_n \, dn \tag{27c}$$

After substituting Eqs.(1) and (5) into Eq.(26), the variation of the work done by the external forces can be written with respect to the bar forces

$$\delta \mathcal{V} = -\int_0^l [\mathcal{P}_z \delta W + \mathcal{V}_x \delta U + \mathcal{M}_y \delta \Psi_y + \mathcal{V}_y \delta V + \mathcal{M}_x \delta \Psi_x + \mathcal{T} \delta \Phi + \mathcal{M}_\omega \delta \Psi_\omega] dz \tag{28}$$

where the bar forces are related to the shell forces as

$$\mathcal{P}_z = \int_s \bar{p}_z ds \tag{29a}$$

$$\mathcal{V}_y = \int_s (\bar{p}_s \sin\theta - \bar{p}_n \cos\theta) ds \tag{29b}$$

$$\mathcal{V}_x = \int_s (\bar{p}_s \cos\theta + \bar{p}_n \sin\theta) ds \tag{29c}$$

$$\mathcal{T} = \int_s (\bar{p}_s r - \bar{p}_n q + \bar{m}_s) ds \tag{29d}$$

$$\mathcal{M}_y = \int_s (\bar{m}_z \sin\theta + \bar{p}_z x) ds \tag{29e}$$

$$\mathcal{M}_x = \int_s (-\bar{m}_z \cos\theta + \bar{p}_z y) ds \tag{29f}$$

$$\mathcal{M}_\omega = \int_s (-\bar{m}_z q + \bar{p}_z \omega) ds \tag{29g}$$

Using the principle that the variation of the total potential energy is zero, the weak form of the present theory for thin-walled composite beams is given by

$$
\begin{aligned}
0 = & \int_0^l \Big[N_z \delta W' + M_y \delta \Psi_y' + M_x \delta \Psi_x' + M_\omega \delta \Psi_\omega' + V_x \delta(U' + \Psi_y) + V_y \delta(V' + \Psi_x) \\
& + T\delta(\Phi' + \Psi_\omega) + M_t \delta(\Phi' - \Psi_\omega) + N_z(U' \delta U' + V' \delta V') \\
& + (M_y - x_p N_z)(V' \delta\Phi' + \Phi' \delta V') - (M_x - y_p N_z)(U' \delta\Phi' + \Phi' \delta U') + (r_p^2 N_z + R_z)\Phi' \delta\Phi' \\
& - \mathcal{P}_z \delta W - \mathcal{V}_x \delta U - \mathcal{M}_y \delta \Psi_y - \mathcal{V}_y \delta V - \mathcal{M}_x \delta \Psi_x - \mathcal{T} \delta\Phi - \mathcal{M}_\omega \delta \Psi_\omega \Big] dz
\end{aligned}
\tag{30}
$$

IV. CONSTITUTIVE EQUATIONS

The constitutive equations of a kth orthotropic lamina in the laminate co-ordinate system of section are given by

$$\left\{ \begin{array}{c} \sigma_z \\ \sigma_{sz} \end{array} \right\}^k = \left[\begin{array}{cc} \bar{Q}_{11}^* & \bar{Q}_{16}^* \\ \bar{Q}_{16}^* & \bar{Q}_{66}^* \end{array} \right]^k \left\{ \begin{array}{c} \epsilon_z \\ \gamma_{sz} \end{array} \right\} \tag{31}$$

where $\bar{Q}_{ij}^*$ are transformed reduced stiffnesses. The transformed reduced stiffnesses can be calculated from the transformed stiffnesses based on the plane stress ($\sigma_s = 0$) and plane strain ($\epsilon_s = 0$) assumption. More detailed explanation can be found in Ref.[26].

The constitutive relation for out-of-plane stress and strain is given by

$$\sigma_{nz} = \bar{Q}_{55}\gamma_{nz} \tag{32}$$

The constitutive equations for bar forces and bar strains are obtained by using Eqs.(18), (23) and (31)

$$
\begin{Bmatrix} N_z \\ M_y \\ M_x \\ M_\omega \\ M_t \\ V_x \\ V_y \\ T \\ R_z \end{Bmatrix} =
\begin{bmatrix}
E_{11} & E_{12} & E_{13} & E_{14} & E_{15} & E_{16} & E_{17} & E_{18} & E_{19} \\
 & E_{22} & E_{23} & E_{24} & E_{25} & E_{26} & E_{27} & E_{28} & E_{29} \\
 & & E_{33} & E_{34} & E_{35} & E_{36} & E_{37} & E_{38} & E_{39} \\
 & & & E_{44} & E_{45} & E_{46} & E_{47} & E_{48} & E_{49} \\
 & & & & E_{55} & E_{56} & E_{57} & E_{58} & E_{59} \\
 & & & & & E_{66} & E_{67} & E_{68} & E_{69} \\
 & & & & & & E_{77} & E_{78} & E_{79} \\
 & & & & & & & E_{88} & E_{89} \\
\text{sym.} & & & & & & & & E_{99}
\end{bmatrix}
\begin{Bmatrix} \epsilon_z^\circ \\ \kappa_y \\ \kappa_x \\ \kappa_\omega \\ \kappa_{sz} \\ \gamma_{xz}^\circ \\ \gamma_{yz}^\circ \\ \gamma_\omega^\circ \\ \chi_z \end{Bmatrix} \tag{33}
$$

where E_{ij} are the laminate stiffnesses of thin-walled composite beams. ($E_{i,9}$ $i = 1..9$) can be defined by

$$E_{19} = \int_s (2rB_{11} + D_{11})ds \tag{34a}$$

$$E_{29} = \int_s \left[2rxB_{11} + D_{11}(x + 2r\sin\theta) + F_{11}\sin\theta\right]ds \tag{34b}$$

$$E_{39} = \int_s \left[2ryB_{11} + D_{11}(y - 2r\cos\theta) - F_{11}\cos\theta\right]ds \tag{34c}$$

$$E_{49} = \int_s \left[2r\omega B_{11} + D_{11}(\omega - 2rq) - F_{11}q\right]ds \tag{34d}$$

$$E_{59} = \int_s \left[2B_{16}r\frac{F}{2t} + D_{16}(\frac{F}{2t} + 2r) + F_{16}\right]ds \tag{34e}$$

$$E_{69} = \int_s (2rB_{16} + D_{16})\cos\theta ds \tag{34f}$$

$$E_{79} = \int_s (2rB_{16} + D_{16})\sin\theta ds \tag{34g}$$

$$E_{89} = \int_s (2rB_{16} + D_{16})(r - \frac{F}{2t})ds \tag{34h}$$

$$E_{99} = \int_s (4r^2 D_{11} + 4rF_{11} + H_{11})ds \tag{34i}$$

where A_{ij}, B_{ij}, D_{ij} matrices are extensional, coupling, bending stiffness and F_{ij}, H_{ij} matrices are the higher order stiffnesses, respectively, defined by

$$(A_{ij}, B_{ij}, D_{ij}, F_{ij}, H_{ij}) = \int \bar{Q}_{ij}(1, n, n^2, n^3, n^4)dn \tag{35}$$

Other values of E_{ij} can be found in Ref.[23]. The explicit forms of the laminate stiffnesses E_{ij} for composite box section are given in the Appendix.

V. GOVERNING EQUATIONS

The nonlinear equilibrium equations of the present study can be obtained by integrating the derivatives of the varied quantities by parts and collecting the coefficients of $\delta W, \delta U, \delta V, \delta \Phi, \delta \Psi_y, \delta \Psi_x$ and $\delta \Psi_\omega$

$$N_z' + \mathcal{P}_z = 0 \tag{36a}$$

$$V_x' + [N_z(U' + y_p\Phi')]' - [M_x\Phi']' + \mathcal{V}_x = 0 \tag{36b}$$

$$V_y' + [N_z(V' - x_p\Phi')]' + [M_y\Phi']' + \mathcal{V}_y = 0 \tag{36c}$$

$$M_t' + T' + [N_z(r_p^2\Phi' + y_pU' - x_pV')]' + [M_yV']' - [M_xU']' + [R_z\Phi']' + \mathcal{T} = 0 \tag{36d}$$

$$M_y' - V_x + \mathcal{M}_y = 0 \tag{36e}$$

$$M_x' - V_y + \mathcal{M}_x = 0 \tag{36f}$$

$$M_\omega' + M_t - T + \mathcal{M}_\omega = 0 \tag{36g}$$

The natural boundary conditions are of the form

$$\delta W \; : \; N_z \tag{37a}$$

$$\delta U \; : \; V_x + N_z(U' + y_p\Phi') - M_x\Phi' \tag{37b}$$

$$\delta V \; : \; V_y + N_z(V' - x_p\Phi') + M_y\Phi' \tag{37c}$$

$$\delta \Phi \; : \; T + M_t + N_z(r_p^2\Phi' + y_pU' - x_pV') + M_yV' - M_xU' + R_z\Phi' \tag{37d}$$

$$\delta \Psi_y \; : \; M_y \tag{37e}$$

$$\delta \Psi_x \; : \; M_x \tag{37f}$$

$$\delta \Psi_\omega \; : \; M_\omega \tag{37g}$$

Eq.(37g) denotes the warping restraint boundary condition. When the warping of the cross section is restrained, $\Psi_\omega = 0$ and when the warping is not restrained, $M_\omega = 0$.

By substituting Eqs.(17) and (33) into Eq.(36), the explicit form of the governing equations can be expressed with respect to the laminate stiffnesses E_{ij}. Eq.(36) is the most general nonlinear equilibrium equations for axial, flexural, torsional and shearing behavior of thin-walled composite beams under various types of loadings, and the dependent variables, $W, U, V, \Phi, \Psi_x, \Psi_y$ and Ψ_ω are fully coupled.

VI. FINITE ELEMENT FORMULATION

The present theory for thin-walled composite beams described in the previous section was implemented via a one-dimensional displacement-based finite element method. **The linear, quadratic and cubic elements with seven degrees of freedom at each node as shown in the Fig.2 are derived. The same interpolation function is used for all the translational and rotational displacements. Reduced integration of shear terms, that is, stiffness coefficients involving laminate stiffnesses ($E_{i,j}$, $i = 6..8, j = 6..8$) is used to avoid shear locking.** The generalized displacements are expressed over each element as a combination of the one-dimensional Lagrange interpolation function $\widehat{\phi_j}$ associated with node j and the nodal values

$$W = \sum_{j=1}^{n} w_j \widehat{\phi_j} \tag{38a}$$

$$U = \sum_{j=1}^{n} u_j \widehat{\phi_j} \tag{38b}$$

$$V = \sum_{j=1}^{n} v_j \widehat{\phi_j} \tag{38c}$$

$$\Phi = \sum_{j=1}^{n} \phi_j \widehat{\phi_j} \tag{38d}$$

$$\Psi_y = \sum_{j=1}^{n} \psi_{yj} \widehat{\phi_j} \tag{38e}$$

$$\Psi_x = \sum_{j=1}^{n} \psi_{xj} \widehat{\phi_j} \tag{38f}$$

$$\Psi_\omega = \sum_{j=1}^{n} \psi_{\omega j} \widehat{\phi_j} \tag{38g}$$

where n is the number of nodes in an element and Lagrange interpolation function $\widehat{\phi_j}$ for linear, quadratic and cubic elements are available in the literature.

Substituting these expressions into the weak statement in Eq.(30), the finite element model of a typical element can be expressed as

$$\left[K(\{\Delta\}) \right]\{\Delta\} = \{f\} \tag{39}$$

The nonlinear algebraic equations of present theory are solved by an iterative method. Thus, the nonlinear equations are linearized by evaluating the nonlinear terms with the known solution from preceding iterations. The Newton−Raphson method that uses the tangent stiffness matrix, which is symmetric for all structural problems,

is used in this study. By using this method, solution of Eq.(39) results in the following linearized equations for the incremental solution at the rth iteration (Reddy [27])

$$[T\{\Delta\}^{r-1}]\{\Delta\} = \{f\} - ([K]\{\Delta\}^{r-1} \tag{40}$$

where the tangent stiffness matrix is defined by

$$T_{ij}^{\alpha\beta} = \frac{\partial K_{ik}^{\alpha\gamma}}{\partial u_j^\beta} u_k^\gamma + K_{ij}^{\alpha\beta} \tag{41}$$

In Eq.(39), $\{\Delta\}$ is the unknown nodal displacements

$$\{\Delta\} = \{W\ U\ V\ \Phi\ \Psi_y\ \Psi_x\ \Psi_\omega\}^{\mathrm{T}} \tag{42}$$

VII. NUMERICAL EXAMPLES

Throughout numerical examples, a tolerance of $\epsilon = 10^{-3}$ and maximum allowable iterations of 20 (per load step) are used to check for convergence of nodal displacements in the Newton−Raphson iteration scheme. **Ten quadratic elements with three nodes are used in the numerical computation**. The initial solution vector is chosen to be the zero vector, so that the first iteration solution corresponds to the linear solution. The results of the present analysis are given for both the linear and nonlinear case.

For verification purpose, a cantilever composite box beam with geometry and stacking sequence shown in Fig.3 under a tip vertical load of 1.78 KN is analyzed. The lamination of this beam consists of eight laminae of equal thickness as follows: $[0/-\theta_2/90]_s$ at the lower flange, $[0/\theta_2/90]_s$ at the upper flange and $[(0/90)_2]_s$ at both webs, respectively. The analysis is carried out assuming both plane stress ($\sigma_s = 0$) and plane strain ($\epsilon_s = 0$) assumptions. The following material properties are used (Stemple and Lee [11]):

$$E_1 = 146.79\mathrm{GPa}\,, E_2 = 10.3\mathrm{GPa}\,, \nu_{12} = 0.28\,, G_{12}\ =\ G_{23} = 6.2\mathrm{GPa}\,, G_{13} = 4.82\mathrm{GPa} \tag{43}$$

The angle of twist and horizontal displacement with respect to fiber angle change are illustrated in Figs.4 and 5. It is clear that horizontal displacement is due solely to coupling-induced geometrical nonlinear effect, which are not present in the linear analysis. Fig.6 reveals that the vertical displacement more than doubles when fiber angle is varied from $\theta = 0°$ to $\theta = 90°$. From the aforementioned figures, the coincidence of the results between Stemple

and Lee [11] and Kalfon and Rand [13] and the present model is observed, while there is the small deviation of the vertical displacement as fiber angle increases. It seems that the solutions in both of the studies [11,13] were calculated by using plane strain assumption. The proposed model agrees well with previously available results and can capture exactly all the geometrical nonlinear response of composite beam.

A pinned-hinged composite box beam of length $L = 2$m under an eccentric uniform load q acting at the midplane of the left web is considered in order to investigate the effect of the load parameter, shear deformation and fiber orientation on the displacements. It is noted earlier by authors [21-25] that the results based on the plane stress assumption ($\sigma_s = 0$) yield better agreement with ABAQUS solution. For this reason, plane stress assumption ($\sigma_s = 0$) is used in numerical computation. The configuration of the composite box beam is shown in Fig.7, and the following engineering constants are used

$$E_1/E_2 = 25, G_{12}/E_2 = 0.6, G_{12} = G_{13} = G_{23}, \nu_{12} = 0.25 \tag{44}$$

For convenience, the following nondimensional values of the axial, vertical displacement, and load parameter are used

$$\overline{w} = \frac{w}{b_1} \tag{45a}$$

$$\overline{v} = \frac{v}{b_1} \tag{45b}$$

$$\overline{q} = \frac{qL^4}{E_2 b_1^3 t} \tag{45c}$$

Stacking sequence of this beam consists of two layers with equal thickness as follows: $[\theta]_2$ at top flange and right web, $[-\theta]_2$ at left web and bottom flange, respectively (Fig.8a). For this lay-up, most coupling stiffnesses become zero, but $E_{17}, E_{18}, E_{19}, E_{25}, E_{35}, E_{28}$ and E_{38} do not vanish due to unsymmetric stacking sequence between the webs and flanges. Accordingly, this beam sustains simultaneously two kinds of couplings from material anisotropy and geometric nonlinearity. As the first example, the stacking sequence at two specific fiber angle $\theta = 45°, 90°$ is considered to investigate the effects of load parameter on the displacements in the high nonlinear region. It should be noted that for $\theta = 90°$, all the coupling stiffness vanish, that is, only geometrical nonlinear effect exists. The load increment of $\Delta\overline{q} = 0.05$ is employed until the first critical point is reached. The results of the linear analysis are also presented to highlight the difference between linear and nonlinear responses with increasing load. Figs.9 and 10 show the load versus vertical displacement and load versus torsional displacement at two fiber angles. It is evident that the linear theory is adequate in a relatively large region up to the point where an applied load reaches value of $\overline{q} = 4$ and 8 for fiber angle $\theta = 90°$ and $45°$, respectively. When comparing with linear analysis, all the nonlinear

displacements increase with increasing value of the load. This is due to the fact that the geometrical nonlinear effect causes axial-flexural-torsional-shearing coupling which results in a decrease in the flexural and torsional stiffness of the beam. The effect of the geometric nonlinearity is apparent with increasing load intensity. The highest load of fiber angle $\theta = 90°$ is smaller than that of $\theta = 45°$. At this load, for $\theta = 45°$, the nonlinear vertical and torsional displacement is about 120% and 350% of the linear value, respectively. It is from Fig.11 that highlights the influence of geometrical nonlinear effect on the axial displacement of beam. This response is never seen in linear analysis because the coupling terms from geometric nonlinearity are not present. It implies that the structure under eccentric transverse load not only causes the vertical displacement and angle of twist as would be observed in linear case, but also causes additional response due solely to geometric nonlinearity never seen in linear case.

To investigate the geometrical nonlinear and shear deformation effects further, the same configuration with the previous example except the load and lay-up is considered. Stacking sequence of the top flange and the right web are $[\theta]_2$, while the bottom flange and the left web are assumed unidirectional (Fig.8b). A constant applied load is analyzed while the fiber angle is rotated in the top flange and the right web. Based on previous numerical example, an applied load $\overline{q} = 7.0$ is chosen to show effect of fiber orientation on the axial-flexural-torsional response. **By using a combination of the one-dimensional linear Lagrange and Hermite-cubic interpolation function in finite element formulation, the results obtained by authors from previous research [24] based on the classical beam theory are also displayed**. The influence of the shear deformation effect is demonstrated by presenting the discrepancy of the vertical and torsional displacements with respect to fiber angle variation in Figs.12 and 13. The nonlinear solutions excluding shear deformation effect remarkably underestimate the displacements for all the range of fiber angles, as expected. As fiber angles are less than $\theta = 30°$, the vertical displacement of linear and nonlinear analysis coincides. The angle of twist of two analyzes shows the same tendency and reaches minimum value between fiber angle $\theta \in [30° - 40°]$, that is, because the torsional rigidity becomes maximum value at this range. However, as the fiber angle increases, since the geometrical nonlinear effect is prominent, the discrepancy between the linear and nonlinear analysis becomes significant. It is observed that the nonlinear vertical displacement is not as sensitive as the nonlinear torsional displacement when fiber angle changes. The difference between displacements of two analyzes is minimum at $\theta = 0°$ and reaches maximum value at $\theta = 90°$. This phenomenon can be explained that the axial, flexural, torsional and shearing rigidities decrease significantly with increasing fiber angle, and thus, the relative geometrical nonlinear effect becomes larger for higher fiber angles.

VIII. CONCLUDING REMARKS

A geometrically nonlinear analysis for thin-walled composite beams with arbitrary lay-ups under various types of loadings has been presented. This model is based on the first-order shear deformable beam theory, and accounts for all the structural coupling coming from both material anisotropy and geometric nonlinearity. General nonlinear governing equations are derived and solved by means of an incremental Newton−Raphson method. A displacement-based one-dimensional finite element model that accounts for the geometric nonlinearity in the von Kármán sense is developed. Numerical results are obtained to investigate the effects of shear deformation, geometric nonlinearity, fiber orientation and load parameter on axial-flexural-torsional response. The shear effects become significant for lower span-to-height ratio and higher degrees of orthotropy of the beam. The present model is found to be appropriate and efficient in analyzing geometrically nonlinear behavior of thin-walled composite beams.

Appendix

The explicit forms of the laminate stiffnesses E_{ij} for composite box section in Fig.14 can be defined by

$$E_{19} = (-2x_1 + 2x_p)B_{11}^1 b_1 + D_{11}^1 b_1 + (-2y_2 + 2y_p)B_{11}^2 b_2 + D_{11}^2 b_2$$
$$+ (2x_3 - 2x_p)B_{11}^3 b_1 + D_{11}^3 b_1 + (2y_4 - 2y_p)B_{11}^4 b_2 + D_{11}^4 b_2 \tag{46a}$$

$$E_{29} = (-2x_1 + 2x_p)x_1 B_{11}^1 b_1 + D_{11}^1 (3x_1 - 2x_p)b_1 - F_{11}^1 b_1$$
$$+ \frac{1}{2}\left[(-2y_2 + 2y_p)B_{11}^2 + D_{11}^2\right]b_2^2 + (-2y_2 + 2y_p)x_1 B_{11}^2 b_2 + D_{11}^2 x_1 b_2$$
$$+ (2x_3 - 2x_p)x_3 B_{11}^3 b_1 + D_{11}^3 (3x_3 - 2x_p)b_1 + F_{11}^3 b_1$$
$$+ \frac{1}{2}\left[(-2y_4 + 2y_p)B_{11}^4 - D_{11}^4\right]b_2^2 + (2y_4 - 2y_p)x_3 B_{11}^4 b_2 + D_{11}^4 x_3 b_2 \tag{46b}$$

$$E_{39} = \frac{1}{2}\left[(2x_1 - 2x_p)B_{11}^1 - D_{11}^1\right]b_1^2 + (-2x_1 + 2x_p)y_4 B_{11}^1 b_1 + D_{11}^1 y_4 b_1$$
$$+ (-2y_2 + 2y_p)y_2 B_{11}^2 b_2 + D_{11}^2 (3y_2 - 2y_p)b_2 - F_{11}^2 b_2$$

$$+ \frac{1}{2}\left[(2x_3 - 2x_p)B_{11}^3 + D_{11}^3\right]b_1^2 + (2x_3 - 2x_p)y_2 B_{11}^3 b_1 + D_{11}^3 y_2 b_1$$

$$+ (2y_4 - 2y_p)y_4 B_{11}^4 b_2 + D_{11}^4 (3y_4 - 2y_p)b_2 + F_{11}^4 b_2 \tag{46c}$$

$$E_{49} = \frac{1}{2}\left[(-2x_1 + 2x_p)A_1 B_{11}^1 + D_{11}^1(A_1 + 2x_1 - 2x_p) - F_{11}^1\right]b_1^2 + (-2x_1 + 2x_p)CB_{11}^1 b_1$$

$$+ D_{11}^1(C - (-2x_1 + 2x_p)(-y_4 + y_p))b_1 - F_{11}^1(-y_4 + y_p)b_1$$

$$+ \frac{1}{2}\left[(-2y_2 + 2y_p)A_2 B_{11}^2 + D_{11}^2(A_2 + 2y_2 - 2y_p) - F_{11}^2\right]b_2^2 + (-2y_2 + 2y_p)(A_1 b_1 + C)B_{11}^2 b_2$$

$$+ D_{11}^2(A_1 b_1 + C - (-2y_2 + 2y_p)(x_1 - x_p))b_2 - F_{11}^2(x_1 - x_p)b_2$$

$$+ \frac{1}{2}\left[(2x_3 - 2x_p)A_3 B_{11}^3 + D_{11}^3(A_3 - 2x_3 + 2x_p) - F_{11}^3\right]b_1^2 + (2x_3 - 2x_p)(A_1 b_1 + A_2 b_2 + C)B_{11}^3 b_1$$

$$+ D_{11}^3(-(2x_3 - 2x_p)(y_2 - y_p) + A_1 b_1 + A_2 b_2 + C)b_1 - F_{11}^3(y_2 - y_p)b_1$$

$$+ \frac{1}{2}\left[(2y_4 - 2y_p)A_4 B_{11}^4 + D_{11}^4(A_4 - 2y_4 + 2y_p) - F_{11}^4\right]b_2^2 + (2y_4 - 2y_p)(C + A_1 b_1 + A_2 b_2 + A_3 b_1)B_{11}^4 b_2$$

$$+ D_{11}^4(C + A_1 b_1 + A_2 b_2 + A_3 b_1 - (2y_4 - 2y_p)(-x_3 + x_p))b_2 - F_{11}^4(-x_3 + x_p)b_2 \tag{46d}$$

$$E_{59} = \frac{1}{2}(-x_1 + x_p)\frac{F}{2t_1}B_{16}^1 b_1 + D_{16}^1\left(\frac{F}{2t_1} - 2x_1 + 2x_p\right)b_1 + F_{16}^1 b_1$$

$$+ \frac{1}{2}(-y_2 + y_p)\frac{F}{2t_2}B_{16}^2 b_2 + D_{16}^1\left(\frac{F}{2t_2} - 2y_2 + 2y_p\right)b_2 + F_{16}^2 b_2$$

$$+ \frac{1}{2}(x_3 - x_p)\frac{F}{2t_3}B_{16}^3 b_1 + D_{16}^3\left(\frac{F}{2t_3} + 2x_3 - 2x_p\right)b_1 + F_{16}^3 b_1$$

$$+ \frac{1}{2}(y_4 - y_p)\frac{F}{2t_4}B_{16}^4 b_2 + D_{11}^4\left(\frac{F}{2t_4} + 2y_4 - 2y_p\right)b_2 + F_{16}^4 b_2 \tag{46e}$$

$$E_{69} = (-2y_2 + 2y_p)B_{16}^2 b_2 + D_{16}^2 b_2 - (2y_4 - 2y_p)B_{16}^4 b_2 - D_{16}^4 b_2 \tag{46f}$$

$$E_{79} = (2x_1 - 2x_p)B_{16}^1 b_1 - D_{16}^1 b_1 + (2x_3 - 2x_p)B_{16}^3 b_1 + D_{16}^3 b_1 \tag{46g}$$

$$E_{89} = \left[(-2x_1 + 2x_p)B_{16}^1 + D_{16}^1\right]\left(-x_1 + x_p - \frac{F}{2t_1}\right)b_1$$

$$+ \left[(-2y_2 + 2y_p)B_{16}^2 + D_{16}^2\right]\left(-y_2 + y_p - \frac{F}{2t_2}\right)b_2$$

$$+ \left[(2x_3 - 2x_p)B_{16}^3 + D_{16}^3\right]\left(x_3 - x_p - \frac{F}{2t_3}\right)b_1$$

$$+ \left[(2y_4 - 2y_p)B_{16}^4 + D_{16}^4\right]\left(y_4 - y_p - \frac{F}{2t_4}\right)b_2 \tag{46h}$$

$$E_{99} = (-4x_1 + 4x_p)(-x_1 + x_p)D_{11}^1 b_1 + (-4x_1 + 4x_p)F_{11}^1 b_1 + H_{11}^1 b_1$$

$$+ (-4y_2 + 4y_p)(-y_2 + y_p)D_{11}^2 b_2 + (-4y_2 + 4y_p)F_{11}^2 b_2 + H_{11}^2 b_2$$

$$+ (4x_3 - 4x_p)(x_3 - x_p)D_{11}^3 b_1 + (4x_3 - 4x_p)F_{11}^3 b_1 + H_{11}^3 b_1$$

$$+ (4y_4 - 4y_p)(y_4 - y_p)D_{11}^4 b_2 + (4y_4 - 4y_p)F_{11}^4 b_2 + H_{11}^4 b_2 \tag{46i}$$

where the St. Venant circuit shear flow F, constant C and other values of E_{ij} can be found in Refs.[22,23]

References

[1] V. Z. Vlasov, Thin Walled Elastic Beams, Israel Program for Scientific Transactions, Jerusalem, 1961.

[2] A. Gjelsvik, The theory of thin walled bars, Wiley, New York, 1981.

[3] A. R. Atilgan, D. H. Hodges, A geometrically nonlinear analysis for nonhomogeneous, anisotropic beams, in: AIAA Paper No.89-1264-CPMobile, AL, Proc. 30th AIAA/ASME/ASCE/ASH/ACS Structures, Structural Dynamics and Materials Conf., 1989.

[4] D. H. Hodges, A. R. Atilgan, C. E. Cesnik, M. V. Fulton, On a simplified strain energy function for geometrically nonlinear behaviour of anisotropic beams, Compos Eng 2 (5-7) (1992) 513 – 526.

[5] C. E. S. Cesnik, D. H. Hodges, A new concept for composite rotor blade cross-sectional modeling, J Am Helicopter Soc 42(1) (1997) 27–38.

[6] C. E. S. Cesnik, S. Shin, On the modeling of integrally actuated helicopter blades, Int J Solids Struct 38 (10-13) (2001) 1765 – 1789.

[7] V. V. Volovoi, D. H. Hodges, C. E. S. Cesnik, B. Popescu, Assessment of beam modeling methods for rotor blade applications, Math Comput Model 33 (10-11) (2001) 1099 – 1112.

[8] W. Yu, D. H. Hodges, V. V. Volovoi, E. D. Fuchs, A generalized Vlasov theory for composite beams, Thin-Walled Struct 43 (9) (2005) 1493 – 1511.

[9] S. M. Jeon, M. H. Cho, I. Lee, Static and dynamic analysis of composite box beams using large deflection theory, Comput Struct 57 (4) (1995) 635 – 642.

[10] N. R. Bauld, L. S. Tzeng, A Vlasov theory for fiber-reinforced beams with thin-walled open cross sections, Int J Solids Struct 20 (3) (1984) 277 – 297.

[11] A. D. Stemple, S. W. Lee, A finite element model for composite beams undergoing large deflection with arbitrary cross-sectional warping., Int J Numer Meth Eng 28 (9) (1989) 2143–2160.

[12] A. D. Stemple, S. W. Lee, Large Deflection Static and Dynamic Finite Element Analysis of Composite Beams with Arbitrary Cross-Sectional Warping, AIAA Paper (1989) 1788–1798.

[13] J. P. Kalfon, O. Rand, Nonlinear analysis of composite thin-walled helicopter blades, Comput Struct 48 (1) (1993) 51 – 61.

[14] P. F. Pai, A. H. Nayfeh, A fully nonlinear theory of curved and twisted composite rotor blades accounting for warpings and three-dimensional stress effects, Int J Solids Struct 31 (9) (1994) 1309 – 1340.

[15] K. Bhaskar, L. Librescu, A geometrically non-linear theory for laminated anisotropic thin-walled beams, Int J Eng Sci 33 (9) (1995) 1331 – 1344.

[16] L. Librescu, O. Song, Thin-Walled Composite Beams: Theory and Application (Solid Mechanics and Its Applications), 1st

Edition, Springer, 2006.

[17] S. P. Machado, V. H. Cortinez, Non-linear model for stability of thin-walled composite beams with shear deformation, Thin-Walled Struct 43 (10) (2005) 1615 – 1645.

[18] V. H. Cortinez, M. T. Piovan, Stability of composite thin-walled beams with shear deformability, Comput Struct 84 (15-16) (2006) 978 – 990.

[19] S. P. Machado, Geometrically non-linear approximations on stability and free vibration of composite beams, Eng Struct 29 (12) (2007) 3567 – 3578.

[20] E. J. Sapountzakis, D. G. Panagos, Shear deformation effect in non-linear analysis of composite beams of variable cross section, Int J Nonlinear Mech 43(7) (2008) 660–682.

[21] J. Lee, Lateral buckling analysis of thin-walled laminated composite beams with monosymmetric sections, Eng Struct 28 (14) (2006) 1997 – 2009.

[22] T. P. Vo, J. Lee, Flexural-torsional behavior of thin-walled closed-section composite box beams, Eng Struct 29 (8) (2007) 1774 – 1782.

[23] T. P. Vo, J. Lee, Flexural-torsional behavior of thin-walled composite box beams using shear-deformable beam theory, Eng Struct 30 (7) (2008) 1958 – 1968.

[24] T. P. Vo, J. Lee, Geometrically nonlinear analysis of thin-walled composite box beams, Comput Struct 87 (3-4) (2009) 236 – 245.

[25] T. P. Vo, Linear and nonlinear finite element analysis of thin-walled composite structures, Ph.D. thesis, Sejong University, Seoul, South Korea (2009).

[26] R. M. Jones, Mechanics of Composite Materials, Taylor & Francis, 1999.

[27] J. N. Reddy, An Introduction to Nonlinear Finite Element Analysis, Oxford University Press, 2004.
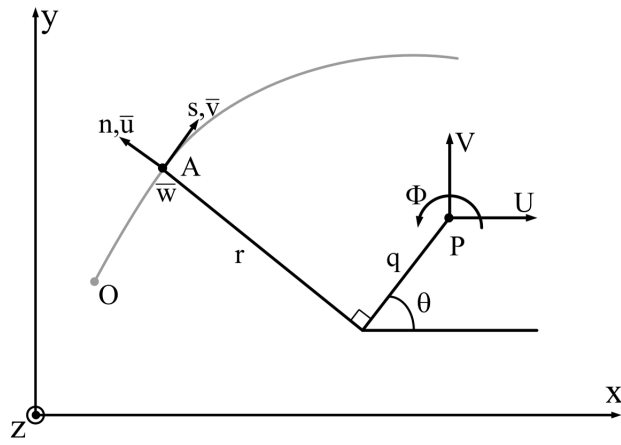
CAPTIONS OF FIGURES

Figure 1: Definition of coordinates and generalized displacements in thin-walled closed sections.
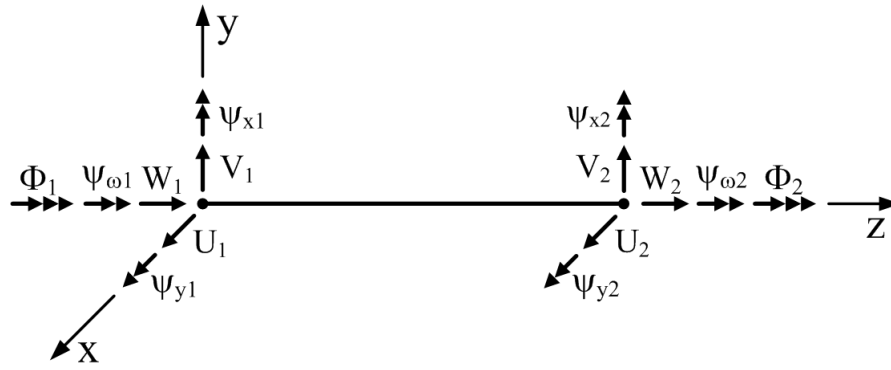
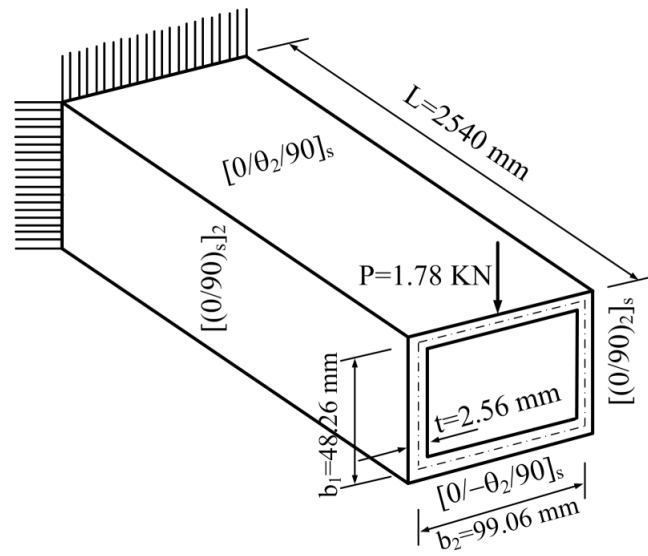Figure 2: Nodal displacements of thin-walled beam element.

Figure 3: A cantilever composite box beam under a 1.78 KN tip vertical load.

Figure 4: Variation of the angle of twist with respect to fiber angle change in the flanges of a cantilever composite box beam under a 1.78 KN tip vertical load.

Figure 5: Variation of the horizontal displacement with respect to fiber angle change in the flanges of a cantilever composite box beam under a 1.78 KN tip vertical load.

Figure 6: Variation of the vertical displacement with respect to fiber angle change in the flanges of a cantilever composite box beam under a 1.78 KN tip vertical load.

Figure 7: A pinned-hinged composite box beam under an eccentric uniform load.

Figure 8: The stacking sequences of thin-walled composite box beams.

Figure 9: Load versus the vertical displacement at mid-span of a pinned-hinged composite box beam under an eccentric uniform load.

Figure 10: Load versus the angle of twist at mid-span of a pinned-hinged composite box beam under an eccentric uniform load.

Figure 11: Load versus the axial displacement at mid-span of a pinned-hinged composite box beam under an eccentric uniform load.

Figure 12: Variation of the vertical displacement at mid-span with respect to fiber angle change in the top flange and right web of a pinned-hinged composite box beam under an eccentric uniform load.

Figure 13: Variation of the angle of twist at mid-span with respect to fiber angle change in the top flange and right web of a pinned-hinged composite box beam under an eccentric uniform load.

Figure 14: Geometry of thin-walled composite box section.

FIG. 1 Definition of coordinates and generalized displacements in thin-walled closed sections.

FIG. 2 Nodal displacements of thin-walled beam element.

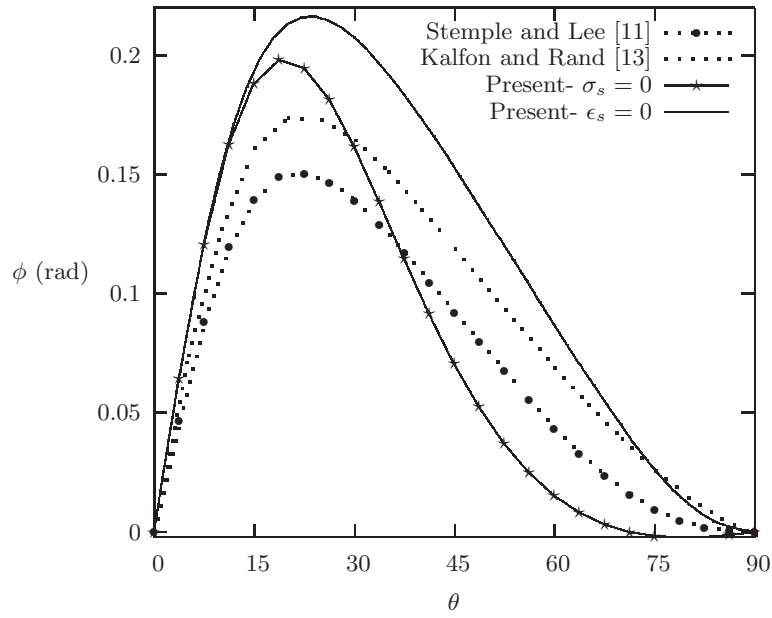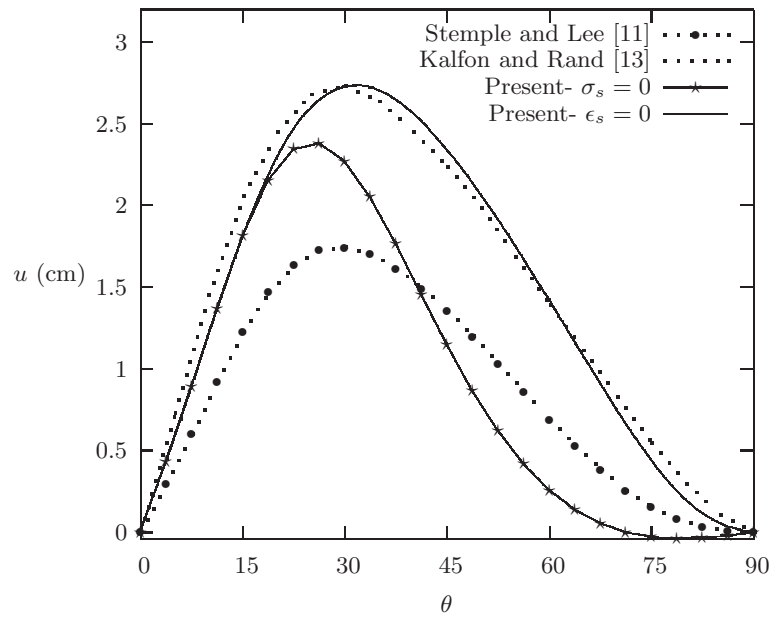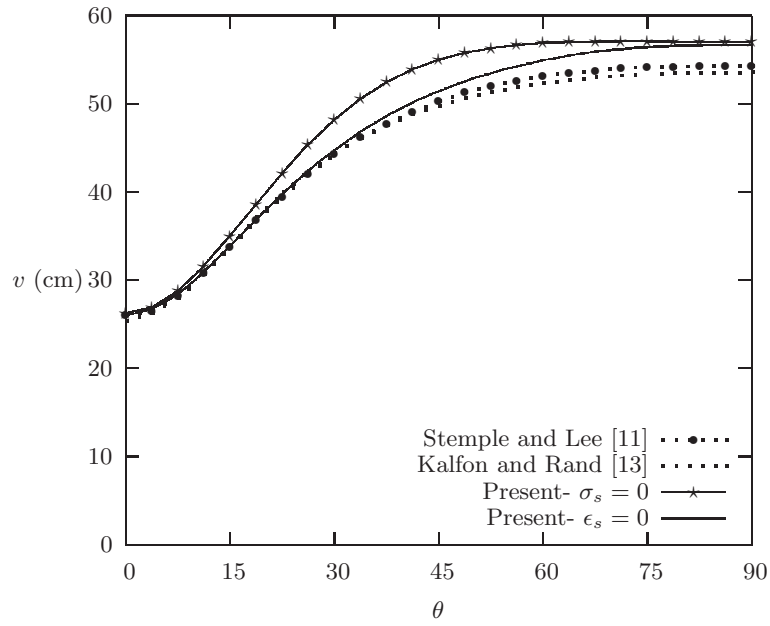FIG. 3 A cantilever composite box beam under a 1.78 KN tip vertical load.

FIG. 4 Variation of the angle of twist with respect to fiber angle change in the flanges of a cantilever composite box beam under a 1.78 KN tip vertical load.

FIG. 5 Variation of the horizontal displacement with respect to fiber angle change in the flanges of a cantilever composite box beam under a 1.78 KN tip vertical load.

FIG. 6 Variation of the vertical displacement with respect to fiber angle change in the flanges of a cantilever composite box beam under a 1.78 KN tip vertical load.
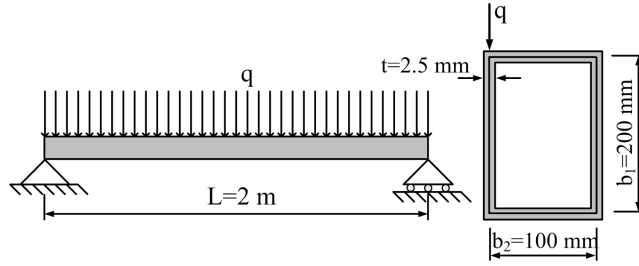
FIG. 7 A pinned-hinged composite box beam under an eccentric uniform load.
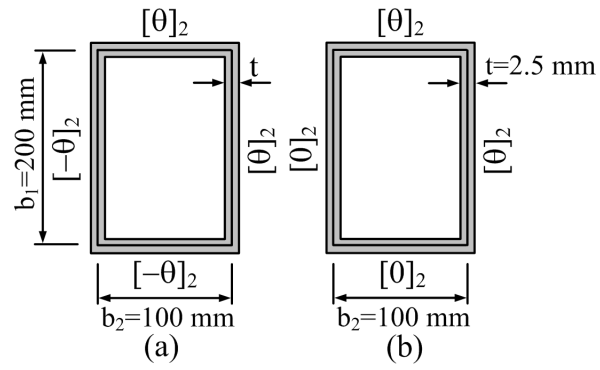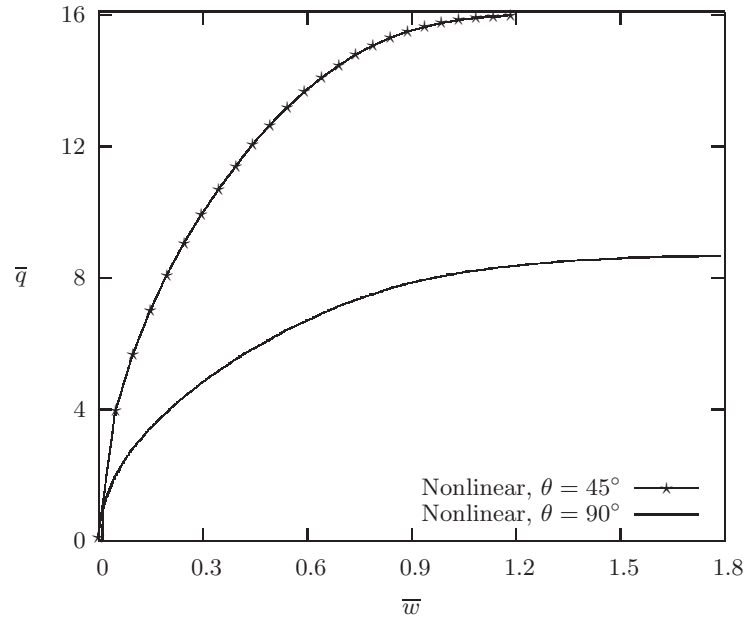
FIG. 8 The stacking sequences of thin-walled composite box beams.
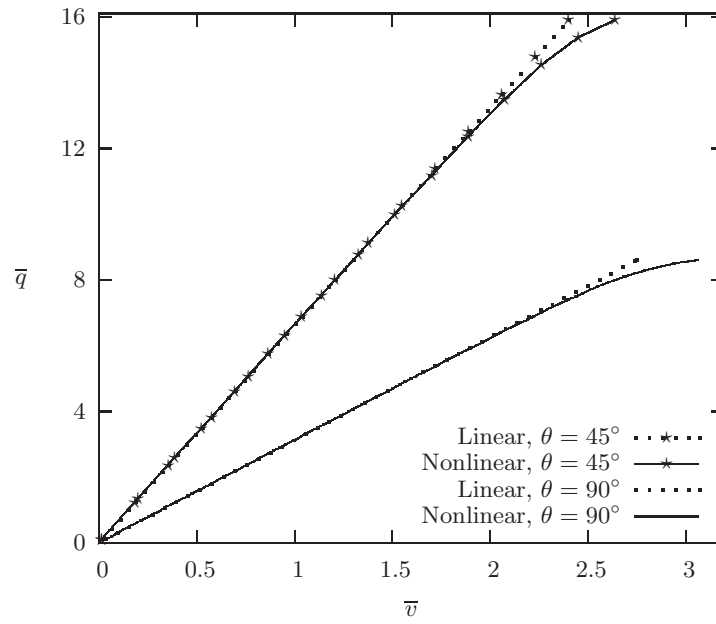
FIG. 9 Load versus the vertical displacement at mid-span of a pinned-hinged composite box beam under an eccentric uniform load.
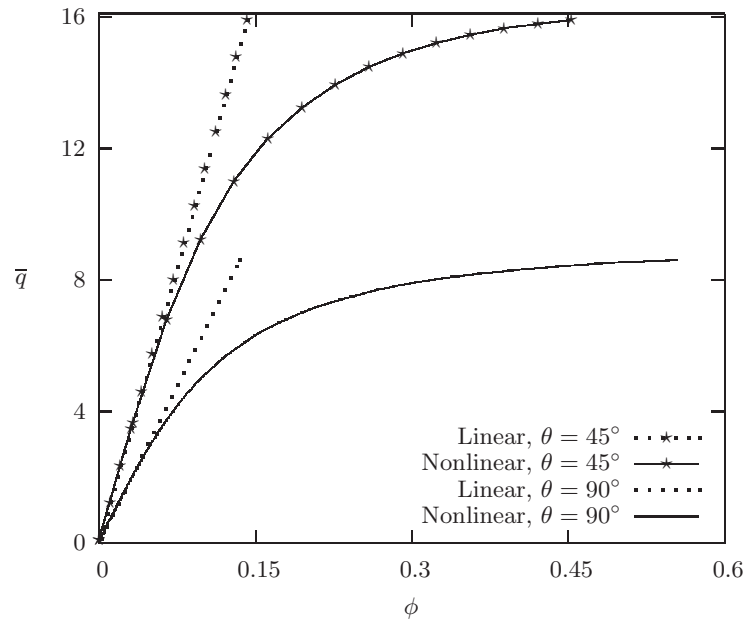
FIG. 10 Load versus the angle of twist at mid-span of a pinned-hinged composite box beam under an eccentric uniform load.

FIG. 11 Load versus the axial displacement at mid-span of a pinned-hinged composite box beam under an eccentric uniform load.
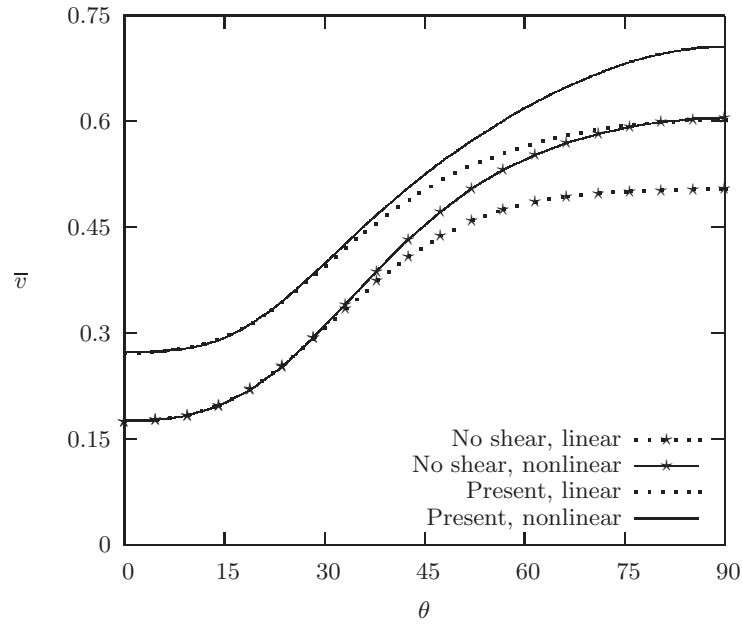
FIG. 12 Variation of the vertical displacement at mid-span with respect to fiber angle change in the top flange and right web of a pinned-hinged composite box beam under an eccentric uniform load.
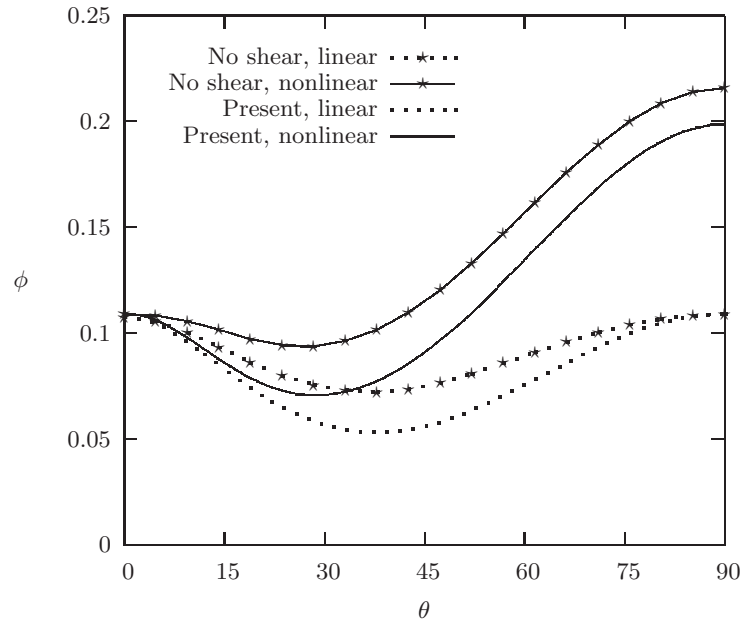
FIG. 13 Variation of the angle of twist at mid-span with respect to fiber angle change in the top flange and right web of a pinned-hinged composite box beam under an eccentric uniform load.
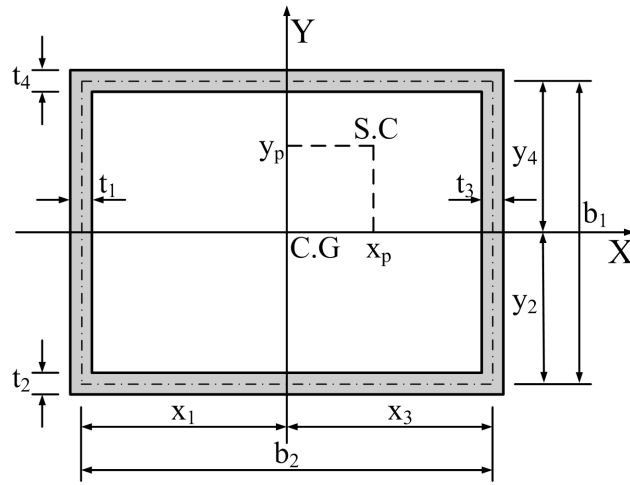
FIG. 14 Geometry of thin-walled composite box section.